

**Spectrum of  $\pi$  electrons in bilayer graphene nanoribbons and nanotubes: An analytical approach**

J. Ruseckas\* and G. Juzeliūnas

*Institute of Theoretical Physics and Astronomy, Vilnius University, LT-01108 Vilnius, Lithuania*

I. V. Zozoulenko

*Solid State Electronics, ITN, Linköping University, SE-601 74 Norköping, Sweden*

(Received 8 October 2010; published 10 January 2011)

We present an analytical description of  $\pi$  electrons of a finite-size bilayer graphene within a framework of the tight-binding model. The bilayered structures considered here are characterized by a rectangular geometry and have a finite size in one or both directions with armchair- and zigzag-shaped edges. We provide an exact analytical description of the spectrum of  $\pi$  electrons in the zigzag and armchair bilayer graphene nanoribbons and nanotubes. We analyze the dispersion relations, the density of states, and the conductance quantization.

DOI: [10.1103/PhysRevB.83.035403](https://doi.org/10.1103/PhysRevB.83.035403)

PACS number(s): 73.22.Pr

**I. INTRODUCTION**

Since its isolation in 2004, graphene—a single sheet of carbon atoms arranged in a honeycomb lattice—has attracted enormous attention because of its highly unusual electronic and transport properties, which are strikingly different from those of conventional semiconductor-based two-dimensional electronic systems (for a review see Refs. 1–4). The significance and potential impact of this new material for electronics was immediately realized. So far, it has been demonstrated that graphene has the highest carrier mobility at room temperature of any known material.<sup>5</sup> However, graphene is a semimetal with no gap and zero density of states at the Fermi energy. This makes it difficult to utilize it in electronic devices such as field-effect transistor (FET) requiring a large on/off current ratio. The energy gap can be opened in a bilayer graphene by applying a gate voltage between the layers.<sup>6</sup> This gate-induced bandgap was demonstrated by Oostinga *et al.*,<sup>7</sup> and the on/off current ratio of around 100 at room temperature for a dual-gate bilayer graphene FET was reported by IBM.<sup>8</sup>

Another way to introduce the gap is to form graphene into nanoribbons.<sup>9,10</sup> The conductance of graphene nanoribbons (GNRs) with lithographically etched edges indeed revealed the gap in the transport measurements.<sup>11,12</sup> This gap has been subsequently understood as the edge-disorder-induced transport gap<sup>13–15</sup> rather than the intrinsic energy gap expected in ideal GNRs due to the confinement<sup>9</sup> or electron interactions and edge effects.<sup>10</sup> In the last few years great progress has been made in fabrication and patterning of GNRs with ultra-smooth and/or atomically controlled edges. This includes, e.g., controlled formation of edges by Joule heating,<sup>16</sup> unzipping carbon nanotubes to form nanoribbons,<sup>17,18</sup> a chemical route to produce nanoribbons with ultrasoft edges,<sup>19</sup> and atomically precise bottom-up fabrication of GNRs.<sup>20</sup> All these advances in nanoribbons fabrication will hopefully soon allow electronic measurements in near-perfect nanoribbons free from edge or bulk disorder defects.

An important insight into the electronic properties of graphene and GNRs can be obtained from exact analytical approaches. Analytic calculations for the electronic structure of GNRs have been reported in Refs. 21–25. The electronic structure of bilayer graphene was addressed in Refs. 26–30, where the analytical results were presented (both exact and

perturbative). We are not, however, aware of any analytical treatment of bilayer GNRs. (Note that a numerical study of the magnetoband structure of GNRs was reported in Refs. 31 and 32, and the analytical and numerical treatment of the edge states in bi- and N-layer graphene and GNRs was presented in Refs. 30 and 33). The purpose of the present study is to provide an exact analytical description of the spectrum of  $\pi$  electrons in zigzag and armchair bilayer nanoribbons and nanotubes, including the dispersion relations, the density of states, and the conductance quantization.

The paper is organized as follows: In order to illustrate our method, in Sec. II we present known analytical results for a simpler system, monolayer graphene of a finite size. Subsequently in Sec. III we derive the main analytical expressions for the energy spectrum of finite-size structures of bilayer graphene. These expressions are used in Sec. IV to analyze the energy spectrum of various bilayer graphene structures near the Fermi energy. Finally, Sec. V summarizes our findings.

**II. SINGLE LAYER GRAPHENE**

Analytical expressions for the  $\pi$  electron spectrum in GNRs and graphene nanotubes (GNTs), based on tight-binding model, were provided in Ref. 24. In this section we will rederive the same expressions in an analytically simpler way. Our method more clearly shows the connection between solutions for the infinite sheet of graphene and for the finite-size sheet. In addition, this simpler method will allow us to derive later on analytical expressions of the  $\pi$  electron spectrum for more complex systems, bilayer GNRs and GNTs.

**A. Electron spectrum in infinite sheet of graphene**

First we will consider the  $\pi$ -electron spectrum in an infinite sheet of graphene. The hexagonal structure of graphene is shown in Fig. 1(a). The structure of the graphene can be viewed as a hexagonal lattice with a basis of two atoms per unit cell. The Cartesian components of the lattice vectors  $\mathbf{a}_1$  and  $\mathbf{a}_2$  are  $a(3/2, \sqrt{3}/2)$  and  $a(3/2, -\sqrt{3}/2)$ , respectively. Here  $a \approx 1.42 \text{ \AA}$  is the carbon-carbon distance.<sup>1</sup> The three nearest-neighbor vectors are given by  $\delta_1 = a(1/2, \sqrt{3}/2)$ ,

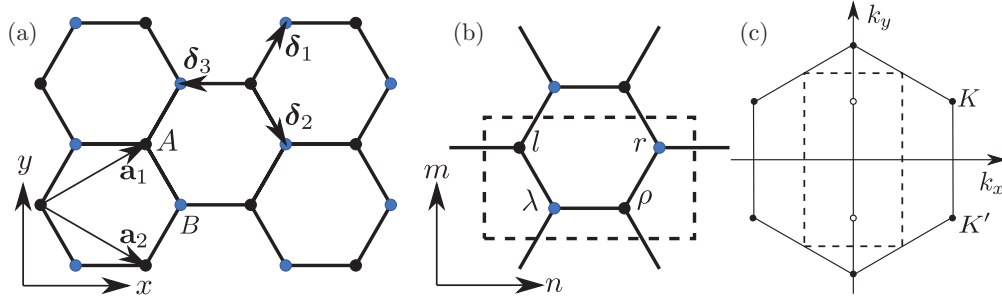


FIG. 1. (Color online) (a) Honeycomb lattice structure of graphene, made out of two interpenetrating triangular lattices;  $\mathbf{a}_1$  and  $\mathbf{a}_2$  are the lattice unit vectors, and  $\delta_i$ ,  $i = 1, 2, 3$ , are the nearest-neighbor vectors. (b) Indication of labels of carbon atoms in the rectangular unit cell. (c) Brillouin zones for hexagonal unit cell (solid hexagon) and rectangular unit cell (dashed rectangle). The Dirac points are indicated by solid circles for the hexagonal unit cell and hollow circles for the rectangular unit cell.

$\delta_2 = a(1/2, -\sqrt{3}/2)$ , and  $\delta_1 = a(-1, 0)$ . The tight-binding Hamiltonian for electrons in graphene has the form

$$H_{\text{gr}} = -t \sum_{(i,j)} (a_i^\dagger b_j + b_j^\dagger a_i), \quad (1)$$

where the operators  $a_i$  and  $b_i$  annihilate an electron on sublattice  $A$  at site  $\mathbf{R}_i^A$  and on sublattice  $B$  at site  $\mathbf{R}_i^B$ , respectively. The parameter  $t$  is the nearest-neighbor hopping energy ( $t \approx 2.8$  eV). From now on we will write all energies in the units of the hopping integral  $t$ ; therefore, we will set  $t = 1$ . Let us label the elementary cells of the lattice with two numbers,  $p$  and  $q$ . Then the atoms in the sublattices  $A$  and  $B$  are positioned at  $\mathbf{R}_{p,q}^A = p\mathbf{a}_1 + q\mathbf{a}_2$  and  $\mathbf{R}_{p,q}^B = \delta_1 + p\mathbf{a}_1 + q\mathbf{a}_2$ , respectively.

The  $\pi$ -electron wave function satisfies the Schrödinger equation,

$$H\Psi = E\Psi. \quad (2)$$

We search for the eigenvectors of the Hamiltonian [Eq. (1)] in the form of plane waves (Bloch states) by taking the probability amplitudes to find an atom in the sites  $\mathbf{R}_{p,q}^A$  and  $\mathbf{R}_{p,q}^B$  of the sublattices  $A$  and  $B$  as

$$\psi_{p,q}^A = c^A e^{i\mathbf{k}\cdot\mathbf{R}_{p,q}^A}, \quad \psi_{p,q}^B = c^B e^{i\mathbf{k}\cdot\mathbf{R}_{p,q}^B}. \quad (3)$$

Thus Eq. (2) yields the following eigenvalue equations for the coefficients  $c^A$  and  $c^B$ :

$$-Ec^A = c^B \tilde{\phi}(\mathbf{k}), \quad (4)$$

$$-Ec^B = c^A \tilde{\phi}(-\mathbf{k}), \quad (5)$$

where

$$\tilde{\phi}(\mathbf{k}) \equiv e^{i\mathbf{k}\cdot\delta_1} + e^{i\mathbf{k}\cdot\delta_2} + e^{i\mathbf{k}\cdot\delta_3}. \quad (6)$$

From Eqs. (4) and (5) we get the eigenenergies and the corresponding coefficients determining the eigenvectors

$$E(\mathbf{k}) = s_1 |\tilde{\phi}(\mathbf{k})|, \quad c^A = -\frac{\tilde{\phi}(\mathbf{k})}{E(\mathbf{k})}, \quad c^B = 1, \quad (7)$$

where  $s_1 = \pm 1$ . In anticipation of rectangular geometry we introduce dimensionless Cartesian components of the wave vector

$$\kappa = 3ak_x, \quad \xi = \sqrt{3}ak_y \quad (8)$$

instead of the wave vector components  $k_x$  and  $k_y$ . Then using the coordinates of the vectors  $\delta_j$  we have

$$\tilde{\phi}(\mathbf{k}) = e^{-i\frac{\kappa}{3}} + 2e^{i\frac{\kappa}{6}} \cos\left(\frac{\xi}{2}\right) \quad (9)$$

and the expression for the eigenenergies becomes<sup>1</sup>

$$E(\mathbf{k}) = s_1 \sqrt{1 + 4 \cos^2\left(\frac{\xi}{2}\right) + 4 \cos\left(\frac{\xi}{2}\right) \cos\left(\frac{\kappa}{2}\right)}. \quad (10)$$

To satisfy boundary conditions it is useful to adopt a larger unit cell characterized by the same geometry as the whole sheet of graphene. Since we are interested in configurations of the graphene with rectangular geometry, we will use a rectangular unit cell, as has been done in Ref. 24. Such a unit cell has four atoms labeled with symbols  $l$ ,  $\lambda$ ,  $\rho$ ,  $r$ , shown in Fig. 1(b). The atoms with labels  $l$  and  $\rho$  belong to the sublattice  $A$ , and the atoms with labels  $\lambda$  and  $r$  belong to the sublattice  $B$ . The position of the unit cell is indicated with two numbers,  $n$  and  $m$ . The first Brillouin zone corresponding to the rectangular unit cell contains the values of the wave vectors  $\kappa$  and  $\xi$  in the intervals  $-\pi \leq \kappa < \pi$ ,  $-\pi \leq \xi < \pi$ . We search for the eigenvectors having the form of plane waves,

$$\psi_{m,n,\alpha} = c_\alpha e^{i\xi m + i\kappa n}, \quad (11)$$

where  $\alpha = l, \rho, \lambda, r$ . This solution can be obtained from Eq. (3) using the equalities

$$c_r = c^B, \quad c_\rho = c^A e^{-i\mathbf{k}\cdot\delta_1}, \quad c_\lambda = c^B e^{-i\mathbf{k}\cdot\mathbf{a}_1}, \quad c_l = c^A e^{-i2ak_x}. \quad (12)$$

The Brillouin zones corresponding to hexagonal and rectangular unit cells are shown in Fig. 1(c). Compared to the area of the Brillouin zone of the hexagonal unit cell, the area of the Brillouin zone of the rectangular unit cell is two times smaller. The smaller Brillouin zone leads to the appearance of additional dispersion branches. Those dispersion branches can be taken into account by using two values of the wave vector  $\kappa$  in Eqs. (10) and (7), one with  $-\pi \leq \kappa < \pi$  and another obtained by replacing  $\kappa$  by  $2\pi + \kappa$ . Using Eqs. (7) and (12) we obtain the coefficients of the eigenvectors

$$c_r = 1, \quad c_\rho = -e^{-i\frac{\xi}{2}} \frac{\phi(\kappa, \xi)}{E(\kappa, \xi)}, \quad (13)$$

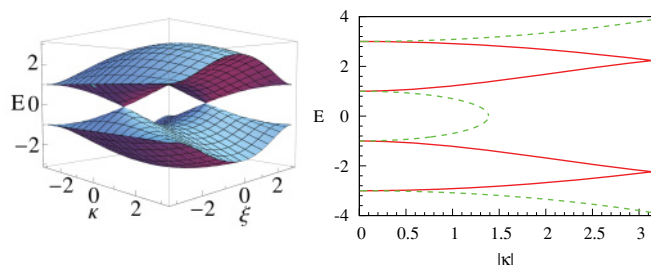


FIG. 2. (Color online) Left: dispersion branches of graphene for rectangular unit cell, calculated according to Eq. (16). Right: dispersion branches for  $\xi = 0$ , showing propagating solutions (red solid) and evanescent solutions (green dashed).

$$c_l = -s_3 e^{-i\frac{\kappa}{2}} \frac{\phi(\kappa, \xi)}{E(\kappa, \xi)}, \quad c_\lambda = s_3 e^{-i\frac{1}{2}(\kappa + \xi)}, \quad (14)$$

where

$$\phi(\kappa, \xi) = s_3 e^{-i\frac{\kappa}{2}} + 2 \cos\left(\frac{\xi}{2}\right), \quad (15)$$

and  $s_3 = \pm 1$  indicates the dispersion branches that appear due to the smaller Brillouin zone. The equation for the energy now becomes

$$E(\kappa, \xi) = s_1 \sqrt{1 + 4 \cos^2\left(\frac{\xi}{2}\right) + s_3 4 \cos\left(\frac{\xi}{2}\right) \cos\left(\frac{\kappa}{2}\right)}. \quad (16)$$

This equation has been obtained in Ref. 24. Zero-energy points of the graphene honeycomb lattice with dispersion relation given by Eq. (10) are at the points  $K = (2\pi, 2\pi/3)$  and  $K' = (2\pi, -2\pi/3)$ , where coordinates are given in  $(\kappa, \xi)$  space.  $K$  points correspond to the corners of the first Brillouin zone. Using the Brillouin zone corresponding to the rectangular unit cell, the zero-energy points have coordinates  $(0, \pm \frac{2\pi}{3})$  and the number of these points is only two, as shown in Fig. 1(c).

Since we will consider finite-size graphene sheets, evanescent solutions become important. Solutions exponentially decreasing or increasing in the  $x$  direction can be obtained by taking  $\kappa = i|\kappa|$  in Eqs. (13), (14), and (16), whereas solutions exponentially decreasing or increasing in the  $y$  direction can be obtained by taking  $\xi = i|\xi|$ . The dependency of the energy on  $\kappa$  when  $\xi = 0$  is shown in Fig. 2. We see that the branches with real and imaginary  $\kappa$  do not intersect at  $|\kappa| > 0$ .

### B. Electron spectrum in various single-layer graphene structures

From the boundary conditions we get restrictions on the possible values of the wave vectors  $\kappa, \xi$ . We will consider the structures of graphene that have a set of  $N$  rectangular unit cells in the  $x$  (armchair) direction and a set of  $N + 1/2$  rectangular unit cells in the  $y$  (zigzag) direction, so that there are  $N$  hexagons along the  $y$  axis. Note that rectangular unit cell shown in Fig. 1(b) extends over the whole hexagon in the  $y$  direction, whereas it extends over more than one hexagon in the  $x$  direction.

Using the periodic boundary condition, corresponding to the graphene torus, we obtain the possible values of the wave vectors  $\kappa, \xi$  as

$$\xi_j = \frac{2\pi}{N} j, \quad j = -\left\lfloor \frac{N}{2} \right\rfloor, -\left\lfloor \frac{N}{2} \right\rfloor + 1, \dots, \left\lfloor \frac{N-1}{2} \right\rfloor \quad (17)$$

$$\kappa_\nu = \frac{2\pi}{N} \nu, \quad \nu = -\left\lfloor \frac{N}{2} \right\rfloor, -\left\lfloor \frac{N}{2} \right\rfloor + 1, \dots, \left\lfloor \frac{N-1}{2} \right\rfloor \quad (18)$$

Here  $\lfloor \cdot \rfloor$  denotes the integer part of a number. Thus the spectrum of a graphene torus is given by Eq. (16) replacing  $\kappa$  and  $\xi$  by  $\kappa_\nu$  and  $\xi_j$ .

For graphene armchair nanotubes one has the periodic boundary condition in the  $x$  direction and the requirement  $\psi_{0,n,r} = \psi_{0,n,l} = \psi_{N+1,n,l} = \psi_{N+1,n,r} = 0$  for the  $y$  direction. Since the energy [Eq. (16)] does not depend on the sign of wave vector  $\xi$ , we will search for the eigenvectors of the Hamiltonian [Eq. (1)] as a superposition of periodic solutions [Eq. (11)] with  $\xi$  and  $-\xi$ ,

$$\psi_{m,n,\alpha} = a c_\alpha(\xi, \kappa_\nu) e^{i\xi m + i\kappa_\nu n} + b c_\alpha(-\xi, \kappa_\nu) e^{-i\xi m + i\kappa_\nu n}, \quad (19)$$

where  $\kappa_\nu$  is given by Eq. (18) and  $\xi$  needs to be determined. From the boundary conditions we get a system of two equations for the coefficients  $a$  and  $b$ :

$$a c_{r,l}(\xi, \kappa_\nu) + b c_{r,l}(-\xi, \kappa_\nu) = 0, \quad (20)$$

$$a e^{i\xi(N+1)} c_{r,l}(\xi, \kappa_\nu) + b e^{-i\xi(N+1)} c_{r,l}(-\xi, \kappa_\nu) = 0. \quad (21)$$

This system of equations has nonzero solutions only when the determinant is zero. From Eqs. (13) and (14) it follows that the coefficients  $c_{r,l}(\xi, \kappa)$  do not depend on the sign of  $\xi$ , and we get the condition  $\sin[\xi(N+1)] = 0$  or

$$\xi = \frac{\pi j}{N+1}, \quad j = 1, \dots, N. \quad (22)$$

Additionally, there are two  $N$ -fold degenerate levels corresponding to  $\xi = \pi$  with energies  $E = \pm 1$ . The states of those levels have zero wave function amplitudes at the  $l$  and  $r$  sites.

For graphene zigzag nanotubes one has the periodic boundary condition in the  $y$  direction and the condition  $\psi_{m,0,r} = \psi_{m,N+1,l} = 0$  for the  $x$  direction. Similar to the armchair nanotubes, the energy [Eq. (16)] does not depend on the sign of wave vector  $\kappa$ , and we search for the eigenvectors of the Hamiltonian [Eq. (1)] as a superposition of periodic solutions [Eq. (11)] with  $\kappa$  and  $-\kappa$ ,

$$\psi_{m,n,\alpha} = a c_\alpha(\xi_j, \kappa) e^{i\xi_j m + i\kappa n} + b c_\alpha(\xi_j, -\kappa) e^{i\xi_j m - i\kappa n}, \quad (23)$$

where  $\xi_j$  is given by Eq. (17) and  $\kappa$  needs to be determined. From the boundary conditions we get a system of two equations for the coefficients  $a$  and  $b$ :

$$a c_r(\xi_j, \kappa) + b c_r(\xi_j, -\kappa) = 0, \quad (24)$$

$$a c_l(\xi_j, \kappa) e^{i\kappa(N+1)} + b c_l(\xi_j, -\kappa) e^{-i\kappa(N+1)} = 0. \quad (25)$$

Using Eqs. (13) and (14) we find that nonzero solutions are possible when

$$\frac{\sin(\kappa N)}{\sin\left[\kappa\left(N + \frac{1}{2}\right)\right]} = -s_3 2 \cos\left(\frac{\xi_j}{2}\right). \quad (26)$$

The possible values of wave vector  $\kappa$  should obey this equation. The same condition has been obtained in Ref. 24. Equation (26) allows for the imaginary values of wave vector  $\kappa$ . The imaginary values appear when  $\xi^c < |\xi_j| < \pi$  and  $s_3 = -1$ , where the critical value  $\xi^c = 2 \arccos[N/(2N+1)]$  of the wave vector  $\xi$  is obtained from Eq. (26) by setting  $\kappa = 0$ . In the limit  $N \rightarrow \infty$  from the condition [Eq. (26)] with imaginary  $\kappa$  and Eq. (16), it follows that  $E = 0$ : edge states near zigzag edges in the semi-infinite system have zero energy.

For an  $N \times \mathcal{N}$  sheet of graphene, open boundary conditions in the  $y$  direction are the same as for armchair nanotubes and in the  $x$  direction are the same as for zigzag nanotubes. Since the resulting conditions for the wave vectors  $\kappa$  and  $\xi$  are not coupled, the eigenvector of the Hamiltonian [Eq. (1)] is a superposition of four periodic solutions having all possible combinations of the signs of  $\kappa$  and  $\xi$  and the possible values of the wave vectors are given by Eqs. (22) and (26). In addition there are two  $N$ -fold degenerate levels corresponding to  $\xi = \pi$  with energies  $E = \pm 1$ .

### III. BILAYER GRAPHENE

Now we will consider the spectrum of  $\pi$  electrons in bilayer graphene. The tight-binding Hamiltonian for electrons in bilayer graphene has the form

$$H_{\text{bi}} = V \sum_j (a_{j,2}^\dagger a_{j,2} + b_{j,2}^\dagger b_{j,2} - a_{j,1}^\dagger a_{j,1} - b_{j,1}^\dagger b_{j,1}) - t \sum_{(i,j),p} (a_{i,p}^\dagger b_{j,p} + b_{j,p}^\dagger a_{i,p}) - t_\perp \sum_j (a_{j,1}^\dagger a_{j,2} + a_{j,2}^\dagger a_{j,1}), \quad (27)$$

where the operators  $a_{i,p}$  and  $b_{i,p}$  annihilate an electron on sublattice  $A_p$  at site  $\mathbf{R}_i^{A_p}$  and on sublattice  $B_p$  at site  $\mathbf{R}_i^{B_p}$ , respectively. The index  $p = 1, 2$  numbers the layers in the bilayer system. In the Hamiltonian [Eq. (27)] we neglected the terms corresponding to the hopping between atom  $B_1$  and atom  $B_2$  with the hopping energy  $\gamma_3$ , and the terms corresponding to the hopping between atom  $A_1$  ( $A_2$ ) and atom  $B_2$  ( $B_1$ ) with the hopping energy  $\gamma_4$ . Neglecting those hopping terms leads to the minimal model of bilayer graphene.<sup>29</sup> The parameter  $t_\perp$  ( $t_\perp \approx 0.4$  eV) is the hopping energy between atom  $A_1$  and atom  $A_2$ , while  $V$  is half the shift in the electrochemical potential between the two layers. As with the monolayer graphene, we will express all the energies in the units of  $t$ .

#### A. Electron spectrum in infinite sheet of bilayer graphene

We will proceed as in the foregoing and will analyze an infinite system at first. The atoms in the sublattices  $A_1$  and  $A_2$  are positioned at  $\mathbf{R}_{p,q}^{A_{1,2}} = p\mathbf{a}_1 + q\mathbf{a}_2$ ; in sublattice  $B_1$  the atoms are positioned at  $\mathbf{R}_{p,q}^{B_1} = \delta_1 + p\mathbf{a}_1 + q\mathbf{a}_2$ ; and in sublattice  $B_2$  the atoms are positioned at  $\mathbf{R}_{p,q}^{B_2} = -\delta_1 + p\mathbf{a}_1 + q\mathbf{a}_2$ . We search for the eigenvectors of the Hamiltonian [Eq. (27)] in the form of plane waves. The probability amplitudes to find

an atom in sites  $\mathbf{R}_{p,q}^{A_{1,2}}$  and  $\mathbf{R}_{p,q}^{B_{1,2}}$  of sublattices  $A_j$  and  $B_j$  are

$$\psi_{p,q}^{A_{1,2}} = c^{A_{1,2}} e^{i\mathbf{k} \cdot \mathbf{R}_{p,q}^{A_{1,2}}}, \quad \psi_{p,q}^{B_{1,2}} = c^{B_{1,2}} e^{i\mathbf{k} \cdot \mathbf{R}_{p,q}^{B_{1,2}}}. \quad (28)$$

The coefficients  $c^{A_p}$  and  $c^{B_p}$  obey the eigenvalue equations

$$-E c^{A_1} = V c^{A_1} + c^{B_1} \tilde{\phi}(\mathbf{k}) + \gamma c^{A_2}, \quad (29)$$

$$-E c^{B_1} = V c^{B_1} + c^{A_1} \tilde{\phi}(-\mathbf{k}), \quad (30)$$

$$-E c^{A_2} = -V c^{A_2} + c^{B_2} \tilde{\phi}(-\mathbf{k}) + \gamma c^{A_1}, \quad (31)$$

$$-E c^{B_2} = -V c^{B_2} + c^{A_2} \tilde{\phi}(\mathbf{k}). \quad (32)$$

Here energy  $E$ , potential  $V$ , and interaction between layers  $\gamma \equiv t_\perp/t$  are in the units of the hopping integral  $t$ . Using the nearest-neighbor hopping energy  $t \approx 2.8$  eV and the hopping energy between two layers  $t_\perp \approx 0.4$  eV one gets  $\gamma \approx 0.14$ . When  $V = 0$ , the  $\pi$ -electron spectrum is determined by the equation

$$E(\mathbf{k}) = s_1 \left( s_2 \frac{\gamma}{2} + \sqrt{\frac{\gamma^2}{4} + |\tilde{\phi}(\mathbf{k})|^2} \right), \quad (33)$$

where  $s_1, s_2 = \pm 1$ . The coefficients of the eigenvector are

$$c^{A_1} = -\frac{E(\mathbf{k})}{\tilde{\phi}(-\mathbf{k})}, \quad c^{B_1} = 1, \\ c^{A_2} = s_1 s_2 \frac{E(\mathbf{k})}{\tilde{\phi}(-\mathbf{k})}, \quad c^{B_2} = -s_1 s_2 \frac{\tilde{\phi}(\mathbf{k})}{\tilde{\phi}(-\mathbf{k})}. \quad (34)$$

When  $V \neq 0$  the spectrum is

$$E(\mathbf{k}) = s_1 \sqrt{\frac{\gamma^2}{2} + V^2 + |\tilde{\phi}(\mathbf{k})|^2} + s_2 \sqrt{\frac{\gamma^4}{4} + |\tilde{\phi}(\mathbf{k})|^2 (4V^2 + \gamma^2)} \quad (35)$$

and the coefficients of the eigenvector are

$$c^{A_1} = -\frac{E(\mathbf{k}) + V}{\tilde{\phi}(-\mathbf{k})}, \quad c^{B_1} = 1, \\ c^{A_2} = \frac{E(\mathbf{k}) - V}{\tilde{\phi}(-\mathbf{k})} f(\mathbf{k}), \quad c^{B_2} = -\frac{\tilde{\phi}(\mathbf{k})}{\tilde{\phi}(-\mathbf{k})} f(\mathbf{k}), \quad (36)$$

where the function

$$f(\mathbf{k}) = \frac{[E(\mathbf{k}) + V]^2 - |\tilde{\phi}(\mathbf{k})|^2}{\gamma[E(\mathbf{k}) - V]} \quad (37)$$

describes the contribution of the second sheet of graphene to the eigenvector.

Finite-size bilayer graphene sheets can be in AB- $\alpha$  or AB- $\beta$  stacking, as is shown in Figs. 3(a) and 3(b). As we did for the graphene monolayer, we will use rectangular unit cells, one shifted with respect to the other, in each layer of bilayer graphene. However, the positions of rectangular cells are different for different stacking types. Rectangular unit cells have eight atoms, with labels  $l_1, \lambda_1, \rho_1, r_1$  and  $l_2, \lambda_2, \rho_2, r_2$ , as shown in Figs. 3(c) and 3(d). For the AB- $\alpha$  stacking, the atoms with labels  $l_1$  and  $\rho_1$  belong to sublattice  $A_1$ , atoms  $\lambda_1$  and  $r_1$  to sublattice  $B_1$ , atoms  $l_2$  and  $\rho_2$  to sublattice  $A_2$ , and atoms  $\lambda_2$  and  $r_2$  to sublattice  $B_2$ . For the AB- $\beta$  stacking the atoms with labels  $l_1$  and  $\rho_1$  belong to sublattice  $B_1$ , atoms

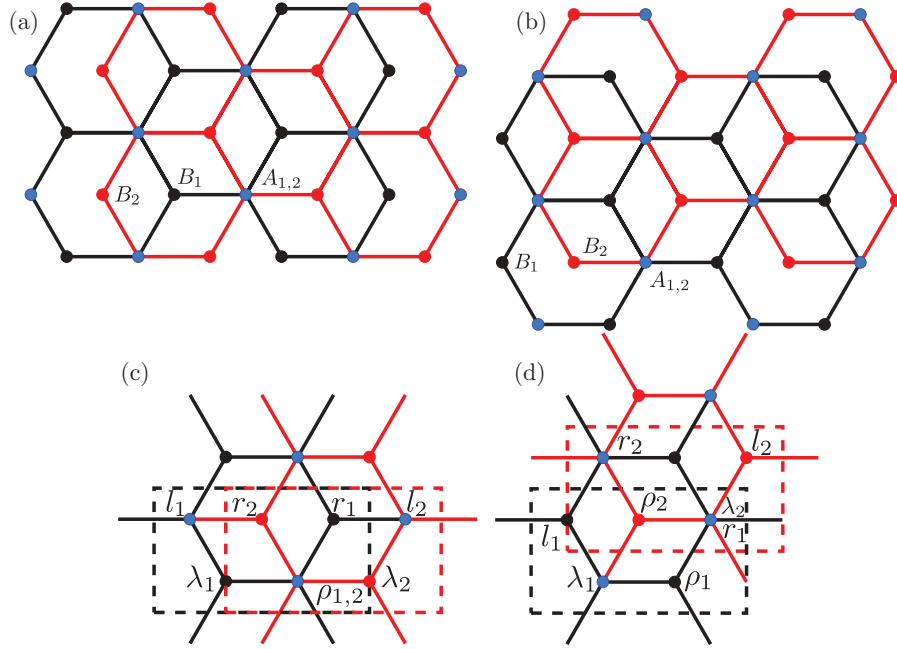


FIG. 3. (Color online) Upper part: sublattices  $A_1$ ,  $A_2$ ,  $B_1$ , and  $B_2$  on bilayer graphene in AB- $\alpha$  stacking (a) and AB- $\beta$  stacking (b). Lower part: indication of labels of carbon atoms used in the description of the  $\pi$ -electron spectrum for bilayer graphene with AB- $\alpha$  stacking (c) and AB- $\beta$  stacking (d).

$\lambda_1$  and  $r_1$  to sublattice  $A_1$ , atoms  $l_2$  and  $\rho_2$  to sublattice  $B_2$ , and atoms  $\lambda_2$  and  $r_2$  to sublattice  $A_2$ .

We search for the solutions of the form

$$\psi_{m,n,\alpha p} = c_{\alpha p} e^{i\xi m + i\kappa n}, \quad (38)$$

where  $\alpha = l, \rho, \lambda, r$  is the label of atoms and  $p = 1, 2$  is the number of the layer. For the AB- $\alpha$  stacking, this solution can be obtained from Eq. (28) using the equalities

$$\begin{aligned} c_{r_1} &= c^{B_1}, & c_{\rho_1} &= c^{A_1} e^{-i\mathbf{k} \cdot \delta_1}, \\ c_{\lambda_1} &= c^{B_1} e^{-i\mathbf{k} \cdot \mathbf{a}_1}, & c_{l_1} &= c^{A_1} e^{-i2a k_x}, \end{aligned} \quad (39)$$

$$\begin{aligned} c_{r_2} &= c^{B_2} e^{-i\mathbf{k} \cdot \mathbf{a}_2}, & c_{\rho_2} &= c^{A_2} e^{-i\mathbf{k} \cdot \delta_1}, \\ c_{\lambda_2} &= c^{B_2} e^{i\mathbf{k} \cdot \delta_2}, & c_{l_2} &= c^{A_2} e^{i a k_x}, \end{aligned} \quad (40)$$

whereas for the AB- $\beta$  stacking the coefficients are

$$\begin{aligned} c_{r_1} &= (c^{A_1})^*, & c_{\rho_1} &= (c^{B_1})^* e^{-i\mathbf{k} \cdot \delta_1}, \\ c_{\lambda_1} &= (c^{A_1})^* e^{-i\mathbf{k} \cdot \mathbf{a}_1}, & c_{l_1} &= (c^{B_1})^* e^{-i2a k_x}, \end{aligned} \quad (41)$$

$$\begin{aligned} c_{r_2} &= (c^{A_2})^* e^{-i\mathbf{k} \cdot \mathbf{a}_2}, & c_{\rho_2} &= (c^{B_2})^* e^{-i a k_x}, \\ c_{\lambda_2} &= (c^{A_2})^*, & c_{l_2} &= (c^{B_2})^* e^{i\mathbf{k} \cdot \delta_1}. \end{aligned} \quad (42)$$

As was the case for monolayer graphene, to take into account the smaller Brillouin zone we need two dispersion branches: one with  $\kappa$  and one with  $2\pi + \kappa$ . Using Eq. (34) or Eq. (36) we obtain the coefficients of the eigenvectors. The expressions for the coefficients are presented in Appendix A. The expression for the energy becomes

$$E(\kappa, \xi) = s_1 \sqrt{\frac{\gamma^2}{2} + V^2 + |\phi(\kappa, \xi)|^2} + s_2 \sqrt{\frac{\gamma^4}{4} + |\phi(\kappa, \xi)|^2 (4V^2 + \gamma^2)}, \quad (43)$$

which reduces to

$$E(\kappa, \xi) = s_1 \left( s_2 \frac{\gamma}{2} + \sqrt{\frac{\gamma^2}{4} + |\phi(\kappa, \xi)|^2} \right) \quad (44)$$

for  $V = 0$ . Here

$$|\phi(\kappa, \xi)|^2 = 1 + 4 \cos^2 \left( \frac{\xi}{2} \right) + s_3 4 \cos \left( \frac{\xi}{2} \right) \cos \left( \frac{\kappa}{2} \right), \quad (45)$$

and  $s_3 = \pm 1$  indicates the dispersion branches that appear due to the smaller Brillouin zone.

In addition to the propagating waves, for finite-size bilayer graphene sheets evanescent solutions become important. Solutions exponentially decreasing or increasing in the  $x$  direction can be obtained by taking  $\kappa = i|\kappa|$ . Solutions exponentially decreasing or increasing in the  $y$  direction can be obtained by taking  $\xi = i|\xi|$ . In addition to the purely imaginary  $\xi$  there are solutions, corresponding to  $s_3 = -1$ , having complex values of  $\xi$ . The dependency of the energy on the wave vector  $\kappa$  when the wave vector  $\xi$  is constant and on the wave vector  $\xi$  when the wave vector  $\kappa$  is constant is shown in Fig. 4. We see that now, in contrast to the graphene monolayer, the branches with real and imaginary  $\kappa$  can have the same energy.

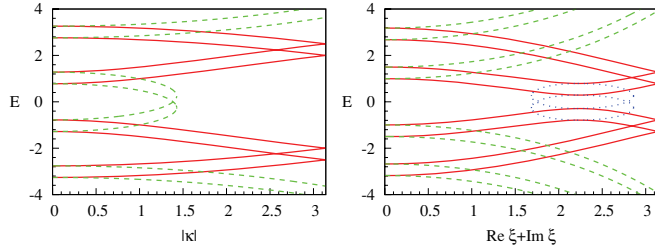


FIG. 4. (Color online) Dispersion branches of bilayer graphene: dependency of the energy on the wave vector  $\kappa$  when the wave vector  $\xi$  is constant ( $\xi = 0$ ) (left) and on the wave vector  $\xi$  when the wave vector  $\kappa$  is constant ( $\kappa = 1.0$ ) (right). Propagating solutions are shown with red solid line, evanescent solutions with green dashed line, and evanescent oscillating solutions with complex value of the wave vector  $\xi$  are shown with blue dotted line. In order to show the structure of the dispersion branches more clearly, the value of the parameter  $\gamma$  is set sufficiently large,  $\gamma = 0.5$ .

### B. Electron spectrum in various bilayer graphene structures

We will consider the structures of bilayer graphene that have a set of  $N$  rectangular unit cells in the  $x$  (armchair) direction and a set of  $\mathcal{N} + 1/2$  rectangular unit cells in the  $y$  (zigzag) direction, so that there are  $\mathcal{N}$  hexagons along the  $y$  axis. Note that the rectangular unit cells shown in Figs. 3(c) and 3(d) extend over the whole hexagon in the  $y$  direction, whereas they extend over more than one hexagon in the  $x$  direction. In principle, in the case of bilayer graphene nanotubes the numbers  $N$  or  $\mathcal{N}$  for the inner and outer cylinders are different. However, for simplicity we will consider them to be the same, which is a good approximation for sufficiently large tubes when  $N \rightarrow \infty$  or  $\mathcal{N} \rightarrow \infty$ .

As we found for the graphene monolayer, from the boundary conditions we get restrictions on the possible values of the wave vectors  $\kappa$  and  $\xi$ . Using a periodic boundary condition corresponding to the bilayer graphene torus, we find that the possible values of the wave vectors  $\kappa$  and  $\xi$  are given by Eqs. (17) and (18).

For bilayer graphene armchair nanotubes one has the periodic boundary condition for the  $x$  direction and the condition

$$\psi_{0,n,r_p} = \psi_{0,n,l_p} = \psi_{\mathcal{N}+1,n,l_p} = \psi_{\mathcal{N}+1,n,r_p} = 0 \quad (46)$$

for the  $y$  direction. Here  $p = 1, 2$  is the number of the layer. This condition is the same for both the AB- $\alpha$  and AB- $\beta$  stackings. For bilayer graphene with AB- $\alpha$  stacking the coefficients  $c_{r_p,l_p}(\xi, \kappa)$  do not depend on the sign of  $\xi$  and we get the same conditions [Eqs. (18) and (22)] for the wave vectors  $\kappa$  and  $\xi$  as we got for the monolayer graphene armchair tubes.

For bilayer graphene with AB- $\beta$  stacking the coefficients  $c_{r_p,l_p}(\xi, \kappa)$  depend on the sign of  $\xi$ , and condition for the possible values of the wave vector  $\xi$  is much more complicated. There are eight boundary conditions in the  $y$  direction. In bilayer graphene there are four eigenstates with different wave vectors along the  $y$  direction,  $\xi^{(1)}$ ,  $\xi^{(2)}$ ,  $\xi^{(3)}$ , and  $\xi^{(4)}$ , having the same energy:  $E(\kappa, \xi^{(1)}) = E(\kappa, \xi^{(2)}) = E(\kappa, \xi^{(3)}) = E(\kappa, \xi^{(4)})$ , as is evident from Fig. 4. Two or four of the wave vectors  $\xi^{(1)}$ ,  $\xi^{(2)}$ ,  $\xi^{(3)}$ , and  $\xi^{(4)}$  can be imaginary or complex numbers. Since the energy does not depend on the sign of  $\xi$ , we can form a wave

function from superposition of eight waves. From the boundary conditions [Eq. (46)], the resulting set of linear equations can have nonzero solutions only if the  $8 \times 8$  determinant is zero. The analytical form of this condition is too large and too complicated to be useful.

For bilayer graphene zigzag nanotubes one has the periodic boundary condition for the  $y$  direction and the condition

$$\psi_{m,0,r_1} = \psi_{m,N+1,l_1} = \psi_{m,0,l_2} = \psi_{m,N+1,r_2} = 0 \quad (47)$$

for the  $x$  direction. Here  $p = 1, 2$  is the number of the layer. This condition is the same for both the AB- $\alpha$  and AB- $\beta$  stackings. In the bilayer graphene there are two eigenstates with wave vectors along the  $x$  direction,  $\kappa^{(1)}$  and  $\kappa^{(2)}$ , having different absolute values but corresponding to the same energy:  $E(\kappa^{(1)}, \xi) = E(\kappa^{(2)}, \xi)$ . One or both of the wave vectors  $\kappa^{(1)}$  and  $\kappa^{(2)}$  can be imaginary. The energy can be equal only if the signs  $s_1, s_2$  obey the condition

$$s_1^{(2)} s_2^{(2)} = -s_1^{(1)} s_2^{(1)} \quad (48)$$

When the bias potential is zero,  $V = 0$ , from the equality of the energy we can express  $\kappa^{(2)}$  as

$$s_3^{(2)} \cos\left(\frac{\kappa^{(2)}}{2}\right) = s_3^{(1)} \cos\left(\frac{\kappa^{(1)}}{2}\right) + s_1^{(1)} s_2^{(1)} \frac{\gamma}{2 \cos\left(\frac{\xi}{2}\right)} E(\kappa^{(1)}, \xi). \quad (49)$$

When  $V \neq 0$ ,

$$s_3^{(2)} \cos\left(\frac{\kappa^{(2)}}{2}\right) = s_3^{(1)} \cos\left(\frac{\kappa^{(1)}}{2}\right) \pm \frac{\gamma}{2 \cos\left(\frac{\xi}{2}\right)} \sqrt{4E^2 V^2 + \gamma^2 (E^2 - V^2)}. \quad (50)$$

There are four boundary conditions in the  $x$  direction. Since the energy does not depend on the sign of  $\kappa$ , we can form a wave function from superposition of four waves. From the boundary conditions [Eq. (47)] the resulting set of linear equations can have nonzero solutions only if the  $4 \times 4$  determinant is zero. The possible values of the wave vector  $\xi$  are given by Eq. (17), and the conditions for the possible values of the wave vector  $\kappa$  are given in Appendix B.

For an  $N \times \mathcal{N}$  sheet of bilayer graphene, open boundary conditions in the  $y$  direction are the same as for armchair nanotubes, Eq. (46), and in the  $x$  direction are the same as for zigzag nanotubes, Eq. (47). For AB- $\alpha$  stacking, the conditions for the possible values of the wave vectors  $\kappa$  and  $\xi$  are a combination of the conditions for zigzag and armchair bilayer graphene tubes. Specifically, when  $V = 0$ , the conditions are given by Eqs. (22) and (B1) or (B2). When  $V \neq 0$ , the conditions are given by Eqs. (22) and (B3). For AB- $\beta$  stacking it is impossible to separate conditions for the wave vector  $\xi$  from the conditions for the wave vector  $\kappa$ . The resulting expressions are very large and complicated.

### C. Summary of the possible values of wave vectors

For structures of bilayer graphene, the energy spectrum is completely determined by Eqs. (44) or (43) with appropriate expressions for wave vectors  $\kappa$  and  $\xi$ .

Equations presented in Appendix B make one quantum number dependent on the other. This dependence appears because of zigzag-shaped edges. For structures where zigzag edges do not exist or their effect can be disregarded, the wave vector  $\kappa_v$  can be replaced by a continuous variable.

Thus, the possible values of wave vectors for various structures are as follows:

1. For the armchair bilayer graphene ribbon of infinite length with AB- $\alpha$  stacking, the wave vectors are determined by

$$0 \leq \kappa \leq \pi, \quad \xi_j = \frac{\pi j}{\mathcal{N} + 1}, \quad j = 1, \dots, \mathcal{N}. \quad (51)$$

2. For the armchair bilayer graphene ribbon of infinite length with AB- $\beta$  stacking we have  $0 \leq \kappa \leq \pi$  and the equation for the possible values of  $\xi$  is complicated.

3. For the zigzag bilayer graphene ribbon of infinite length we have  $0 \leq \xi \leq \pi$ , and the conditions for the possible values of  $\kappa$ , given in Appendix B, are different for AB- $\alpha$  and AB- $\beta$  stackings.

4. For the zigzag bilayer carbon tube of infinite length with AB- $\alpha$  or AB- $\beta$  stacking, the wave vectors are determined by

$$0 \leq \kappa \leq \pi, \quad \xi_j = \frac{2\pi}{\mathcal{N}} j, \quad (52)$$

$$j = -\left\lfloor \frac{\mathcal{N}}{2} \right\rfloor, -\left\lfloor \frac{\mathcal{N}}{2} \right\rfloor + 1, \dots, \left\lfloor \frac{\mathcal{N} - 1}{2} \right\rfloor.$$

5. For the armchair bilayer carbon tube of infinite length with AB- $\alpha$  or AB- $\beta$  stacking,

$$\kappa_v = \frac{2\pi}{N} v, \quad v = -\left\lfloor \frac{N}{2} \right\rfloor, \quad (53)$$

$$-\left\lfloor \frac{N}{2} \right\rfloor + 1, \dots, \left\lfloor \frac{N - 1}{2} \right\rfloor, \quad 0 \leq \xi \leq \pi.$$

Taking into account the ranges of the possible values of the wave vectors, zero-energy points for various structures with bias potential  $V = 0$  are as follows:

6. For zigzag bilayer carbon tube, zero-energy points are  $(0, \frac{2\pi}{3})$ ,  $(0, -\frac{2\pi}{3})$ .

7. For armchair bilayer carbon tube, zero-energy point is  $(0, \frac{2\pi}{3})$ .

8. The dispersion of armchair bilayer graphene ribbon has only one zero-energy point  $(0, \frac{2\pi}{3})$ .

9. For zigzag bilayer graphene ribbon dispersion, this point cannot be shown in the real plane.

#### IV. BAND STRUCTURE NEAR THE FERMI ENERGY

In this Section we focus on only the part of the spectrum with the smallest absolute value of energy. This part corresponds to  $s_2 = -1$ ,  $s_3 = -1$ . In order to obtain an approximate expression for the energy spectrum near the Fermi energy we expand Eq. (45) in a power series near the zero point  $\kappa = 0$ ,

$\xi = 2\pi/3$ , yielding

$$|\phi(\kappa, \xi)|^2 \approx \frac{3}{4} \left[ \frac{\kappa^2}{3} \left( 1 - \frac{\sqrt{3}}{2} q \right) + q^2 \left( 1 + \frac{q}{2\sqrt{3}} \right) \right]$$

$$\approx \frac{3}{4} \left[ \frac{\kappa^2}{3} + \left( q - \frac{\kappa^2}{4\sqrt{3}} \right)^2 \right]. \quad (54)$$

Here  $q \equiv \xi - 2\pi/3$  and  $|\kappa| \ll 1$ ,  $|q| \ll 1$ . Substituting Eq. (54) into Eq. (44) or Eq. (43) one obtains the approximate expression for the energy spectrum. Thus, when the bias potential is zero,  $V = 0$ , the approximate expression for the energy is

$$E(\kappa, \xi) = s_1 \left\{ -\frac{\gamma}{2} + \sqrt{\frac{\gamma^2}{4} + \frac{3}{4} \left[ \frac{\kappa^2}{3} + \left( q - \frac{\kappa^2}{4\sqrt{3}} \right)^2 \right]} \right\} \quad (55)$$

Furthermore, assuming that  $|\phi(\kappa, \xi)|^2 \ll \gamma$ , the branch of Eq. (44) with  $s_2 = -1$ ,  $s_3 = -1$  takes the form

$$E(\kappa, \xi) \approx s_1 \frac{|\phi(\kappa, \xi)|^2}{\gamma}. \quad (56)$$

When  $V \neq 0$  and  $V \ll \gamma$ , then Eq. (43) becomes

$$E(\kappa, \xi) \approx s_1 V - s_1 \frac{2V}{\gamma^2} |\phi(\kappa, \xi)|^2 + s_1 \frac{|\phi(\kappa, \xi)|^4}{2V\gamma^2}. \quad (57)$$

The bilayer graphene has a gap at  $|\phi(\kappa, \xi)|^2 = 2V^2$ . However, since the parameter  $\gamma$  is small,  $\gamma \ll 1$ , the approximate expressions of Eqs. (56) and (57) are suitable only for very small values of  $|\kappa|$  and  $|q|$ .

The spectrum of various structures of bilayer graphene can be obtained from the approximate expressions for  $|\phi(\kappa, \xi)|^2$  near zero points. In contrast to Eqs. (56) and (57), the energy of monolayer graphene is  $E(\kappa, \xi) = s_1 \sqrt{|\phi(\kappa, \xi)|^2}$ . Thus, the analysis of the square root of  $|\phi(\kappa, \xi)|^2$  essentially was done in Ref. 24. Going back to the original wave vectors  $k_x$  and  $k_y$ , the band structure of bilayer graphene tubes and ribbons when  $V = 0$  as in Ref. 24 can be summarized by the equation

$$E_v(k_{\parallel}) \approx s_1 \left( -\frac{\gamma}{2} + \sqrt{\frac{\gamma^2}{4} + \frac{9}{4} a^2 [(k_{\parallel} - \bar{k}_{\parallel}^{\sigma})^2 + k_{\perp v}^{\sigma 2}] } \right), \quad (58)$$

where  $k_{\parallel}$  and  $k_{\perp v}$  denote the longitudinal (continuous) and the transverse (quantized) components of the wave vector, respectively. Index  $\sigma$  specifies the structure. Further in this Section we will consider only the case when  $V = 0$ .

#### A. Quantum conductance

Within the framework of the Landauer approach,<sup>34-37</sup> the zero-temperature conductance of an ideal wire is equal to

$$G(E) = \frac{2e^2}{h} \sum_v g_v T_v(E), \quad (59)$$

where  $2e^2/h$  is conductance quantum,  $g_v$  is the band degeneracy, and transmission coefficient  $T_v$  is 0 or 1 depending on

TABLE I. Degeneracy  $g_v^\sigma$  of the  $\nu$ th band energy  $|E_v^\sigma(k_{\parallel} = 0)|$ 

$\sigma$	$g_v^\sigma$
Armchair bilayer carbon tube	$1(\nu = 0), 2(\nu \neq 0)$
Zigzag bilayer carbon tube	2
Armchair bilayer graphene ribbon	1
Zigzag bilayer graphene ribbon	1

whether the  $\nu$ th band is open or closed for charge carriers with energy  $E$ .

When bias potential is zero,  $V = 0$ , the transmission coefficient is  $T_\nu(E) = \Theta(E - E_v^\sigma)$  for conduction bands and  $T_\nu(E) = \Theta(|E - E_v^\sigma|)$  for valence bands. Here  $E_v^\sigma$  are the subband threshold energies and  $\Theta(x)$  is the Heaviside step function. When the approximation Eq. (58) is valid, the subband threshold energies are

$$E_v^\sigma = s_1 \left( -\frac{\gamma}{2} + \sqrt{\frac{\gamma^2}{4} + \frac{9}{4}a^2k_{\perp\nu}^2} \right). \quad (60)$$

The degeneracies are shown in Table I. The values of  $g_\nu$  for armchair bilayer carbon tube and zigzag bilayer graphene ribbon with  $\nu > 1$ , represented in Table I, should be doubled, because electron or hole states with  $\pm k_{\parallel} \neq 0$  are degenerate.

The electron or hole conductance of armchair and zigzag bilayer carbon tubes and their parent graphene ribbons has thus the form of a ladder, symmetrically ascending with the increase in energy for electrons, and with the decrease of energy for holes. For the charge carrier energy that falls between the  $n$ th and  $(n + 1)$ th bands, the wire conductance equals

$$G(E) = \frac{2e^2}{h} \begin{cases} n & \text{armchair bilayer ribbon,} \\ 2n + 2 & \text{zigzag bilayer ribbon,} \\ 2n & \text{zigzag bilayer carbon tube,} \\ 2(2n + 1) & \text{armchair bilayer carbon tube.} \end{cases} \quad (61)$$

The conductance for bilayer graphene ribbons has been numerically calculated in Ref. 31. Equation (61) for the conductance coincides with that of Ref. 31.

### B. Density of states

The density of states (DOS) of a quantum wire, including a factor 2 for the spin degeneracy, reads

$$\rho(E) = \frac{2}{\pi} \sum_{\nu} \left[ \frac{dE_{\nu}(k_{\parallel}, k_{\perp\nu})}{dk_{\parallel}} \right]^{-1}. \quad (62)$$

The summation includes all transverse modes with energy  $E_{\nu} \leq E$ . Using Eq. (58) we obtain the DOS of bilayer graphene,

$$\rho(E) = \frac{2}{3\pi a} \sum_{\nu} g_{\nu} \frac{(2|E| + \gamma)}{\sqrt{(|E| - |E_{\nu}^{\sigma}|)(|E| + |E_{\nu}^{\sigma}| + \gamma)}} \times \Theta(|E| - |E_{\nu}^{\sigma}|). \quad (63)$$

The index  $\nu$  is  $\nu = 0, \pm 1, \pm 2, \dots$  for bilayer graphene tubes and armchair bilayer graphene ribbons, and  $\nu = 0, 1, 2, \dots$  for zigzag bilayer graphene ribbons. The electron density at zero temperature is obtained by the integration of the DOS from

the charge neutrality point  $\mu_0 = 0$  to the Fermi energy,

$$n = \int_0^{E_F} \rho(E) dE. \quad (64)$$

Using Eq. (63) we get

$$n^{\sigma}(E_F) = \frac{4}{3\pi a} \sum_{\nu} g_{\nu} \sqrt{(|E_F| - |E_{\nu}^{\sigma}|)(|E_F| + |E_{\nu}^{\sigma}| + \gamma)} \times \Theta(|E_F| - |E_{\nu}^{\sigma}|). \quad (65)$$

### C. Armchair bilayer carbon tube

For the armchair bilayer carbon tube we have that  $\kappa$  in Eq. (54) has discrete values  $\kappa_{\nu} = 2\pi\nu/N$ ,  $\nu = 0, \pm 1, \dots$ , and  $q$  is continuous. Thus the energy spectrum has the form

$$E_{\nu}(k_y) = s_1 \left\{ -\frac{\gamma}{2} + \sqrt{\frac{\gamma^2}{4} + \frac{9}{4}a^2 \left[ (k_y - \bar{k}_{y,\nu})^2 + \frac{4\pi^2\nu^2}{9a^2N^2} \right]} \right\}, \quad (66)$$

with

$$\bar{k}_{y,\nu} = \frac{2\pi}{3\sqrt{3}a} + \frac{\pi^2\nu^2}{3aN^2}. \quad (67)$$

Conduction (valence) band bottoms (tops) are equal to

$$E_{\nu} = s_1 \left( -\frac{\gamma}{2} + \sqrt{\frac{\gamma^2}{4} + \frac{\pi^2\nu^2}{N^2}} \right). \quad (68)$$

The distance between the minima of the dispersion branches with the indices  $s_2 = -1$  and  $s_2 = +1$  is  $\gamma$ . The number  $\nu$  of subbands with the index  $s_2 = -1$  and energy smaller than the energies of the subbands with index  $s_2 = +1$  is greater than 1 only when the number of rectangular unit cells in the  $x$  direction,  $N$ , is sufficiently large. Using the equation  $E_{\nu, \max} = \gamma$  and estimating the subband threshold energy [Eq. (68)] as  $E_{\nu} \approx \pi^2\nu^2/(\gamma N^2)$ , one obtains that the requirement  $\nu \gg 1$  leads to  $N \gg \pi/\gamma$ . In calculations we used  $N = 100$ .

The band structure, calculated with exact Eqs. (44) and (45) and approximated according to Eq. (66), is represented in Fig. 5. One sees that Eq. (66) provides a good approximation of the exact results. Also shown is the DOS, calculated with Eqs. (63) and (68), and the conductance  $G(E) = (2e^2/h)2(2n + 1)$ .

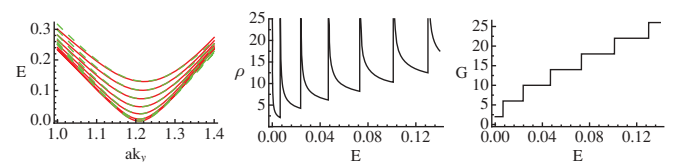


FIG. 5. (Color online) Band structure of armchair bilayer carbon tubes (left), DOS (center), and conductance (right). The number of rectangular unit cells in the  $x$  direction  $N = 100$ . Solid red lines are calculated according to Eqs. (44) and (45); dashed green lines represent the approximation of Eq. (66). Bands with  $s_2 = +1$  are not shown. DOS is given in units of  $a^{-1}$  and is calculated according to Eqs. (63) and (68). The conductance is given in units of  $2e^2/h$  and is calculated using Eq. (61).

#### D. Zigzag bilayer carbon tube

Distinct from armchair bilayer carbon tubes, which are always metallic when  $V = 0$ , zigzag bilayer carbon tube has a gapless spectrum if  $j^* \equiv \mathcal{N}/3$  is an integer,  $E_{j=j^*}(\kappa = 0) = 0$ . Otherwise, the zigzag bilayer carbon tube spectrum has a gap. If  $\mathcal{N}/3$  is not an integer, the band index of the lowest conduction (highest valence) band can be equal either to  $j^* \equiv (\mathcal{N} - 1)/3$  or to  $j^* \equiv (\mathcal{N} + 1)/3$ . As a result of expansion near zero-energy points in powers of  $\kappa$  and  $2\pi(j - j^*)/\mathcal{N}$ , we arrive at

$$|\phi(\kappa, \xi)|^2 \approx \frac{3}{4} \left( q_v^2 + \frac{\kappa^2}{3} \right), \quad (69)$$

where

$$q_v = \begin{cases} \frac{2\pi}{\mathcal{N}} \left| v - \frac{1}{3} \right| \ll 1, & \text{semiconducting,} \\ \frac{2\pi|v|}{\mathcal{N}} \left( 1 + \frac{\pi v}{2\sqrt{3}\mathcal{N}} \right) \ll 1, & \text{metallic,} \end{cases}$$

with  $v = 0, \pm 1, \dots$ . The wave vector component  $\kappa$  is continuous. The energy spectrum has the form

$$E_v(k_x) = s_1 \left[ -\frac{\gamma}{2} + \sqrt{\frac{\gamma^2}{4} + \frac{9}{4}a^2 \left( k_x^2 + \frac{q_v^2}{3a^2} \right)} \right]. \quad (70)$$

Conduction (valence) band bottoms (tops) are equal to

$$E_v = s_1 \left( -\frac{\gamma}{2} + \sqrt{\frac{\gamma^2}{4} + \frac{3}{4}q_v^2} \right). \quad (71)$$

The number  $\nu$  of subbands with the index  $s_2 = -1$  and energy smaller than the energies of the subbands with index  $s_2 = +1$  is greater than 1 only when the number of hexagons in the  $y$  direction  $\mathcal{N}$  is sufficiently large. Approximating Eq. (71) as  $3\pi^2\nu^2/(\gamma\mathcal{N}^2)$  we get  $\mathcal{N} \gg \sqrt{3}\pi/\gamma$ . In calculations we used  $\mathcal{N} = 102$  for metallic tubes and  $\mathcal{N} = 100$  for semiconducting tubes.

The band structure, calculated using exact Eqs. (44) and (45) and approximated according to Eq. (70) for metallic and for semiconducting tubes is shown in Fig. 6. One sees that Eq. (70) provides a good approximation of the exact results. Also shown is the DOS, calculated with Eqs. (63) and (71), and the conductance  $G(E) = (2e^2/h)2n$ .

#### E. Armchair bilayer graphene ribbon

For the armchair bilayer graphene ribbon with AB- $\alpha$  stacking, the condition for the wave-vector component  $\xi$  has a simple expression. When  $V = 0$  and  $j^* \equiv 2(\mathcal{N} + 1)/3$  is an integer, then the armchair bilayer graphene ribbon is metallic. Then index  $\nu = j - j^* = 0$  corresponds to the zero-energy band. If  $2(\mathcal{N} + 1)/3$  is not an integer, the armchair bilayer graphene ribbon spectrum has a gap, and the band closest to zero is either  $j^* \equiv (2\mathcal{N} + 1)/3$  or  $j^* \equiv (2\mathcal{N} + 3)/3$ , depending on which of these two numbers is an integer. For  $\kappa, \nu/\mathcal{N} \ll 1$  we get Eq. (69) with

$$q_v = \begin{cases} \frac{\pi}{\mathcal{N} + 1} \left| v - \frac{1}{3} \right| \ll 1, & \text{semiconducting,} \\ \frac{\pi|v|}{\mathcal{N} + 1} \left( 1 + \frac{\pi v}{4\sqrt{3}(\mathcal{N} + 1)} \right) \ll 1, & \text{metallic,} \end{cases} \quad (72)$$

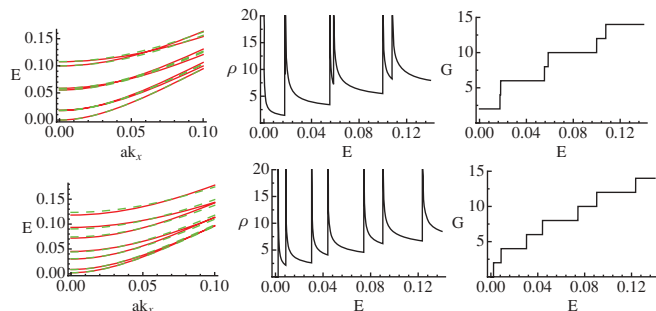


FIG. 6. (Color online) Upper part: band structure of metallic zigzag bilayer carbon tubes (left), DOS (center) and conductance (right). The number of hexagons in the  $y$  direction  $\mathcal{N} = 102$ . Lower part: band structure of semiconducting zigzag bilayer carbon tubes (left), DOS (center) and conductance (right). The number of hexagons in the  $y$  direction  $\mathcal{N} = 100$ . Solid red lines are calculated according to Eqs. (44), (45); dashed green lines represent approximation (70). Bands with  $s_2 = +1$  are not shown. DOS is given in units of  $a^{-1}$  and is calculated according to Eqs. (63), (71). The conductance is given in units of  $2e^2/h$  and is calculated using Eq. (61).

with  $v = 0, \pm 1, \dots$ . The wave vector component  $\kappa$  is continuous. The difference between the boundary conditions for armchair bilayer graphene ribbons and zigzag bilayer graphene tubes results in about two-times smaller band spacing in the armchair ribbon spectrum than was found for the zigzag tube spectrum.

The energy spectrum has the form

$$E_v(k_x) = s_1 \left[ -\frac{\gamma}{2} + \sqrt{\frac{\gamma^2}{4} + \frac{9}{4}a^2 \left( k_x^2 + \frac{q_v^2}{3a^2} \right)} \right]. \quad (73)$$

Conduction (valence) band bottoms (tops) are equal to

$$E_v = s_1 \left( -\frac{\gamma}{2} + \sqrt{\frac{\gamma^2}{4} + \frac{3}{4}q_v^2} \right). \quad (74)$$

The number  $\nu$  of subbands with the index  $s_2 = -1$  and energy smaller than the energies of the subbands with index  $s_2 = +1$  is greater than 1 only when the number of hexagons in the  $y$  direction  $\mathcal{N}$  is sufficiently large. Approximating Eq. (74) as  $3\pi^2\nu^2/4\gamma(\mathcal{N} + 1)^2$  we get  $\mathcal{N} \gg \sqrt{3}\pi/(2\gamma)$ . In calculations we used  $\mathcal{N} = 101$  for metallic ribbons and  $\mathcal{N} = 100$  for semiconducting ribbons.

The band structure, calculated with the use of exact Eqs. (44) and (45) and approximated according to Eq. (73) for metallic and semiconducting ribbons is shown in Fig. 7. One sees that Eq. (73) provides a good approximation of the exact results. Also shown is the DOS, calculated with Eqs. (63) and (74), and the conductance  $G(E) = (2e^2/h)n$ .

For the armchair bilayer graphene ribbon with AB- $\beta$  stacking there are no explicit expressions for the possible values of  $q$ .

#### F. Zigzag bilayer graphene ribbon

In zigzag bilayer graphene ribbons the wave vector component  $q$  is continuous while the possible values of  $\kappa$  are given by the solutions of Eqs. (49) and (B1), plus Eq. (B2) for AB- $\alpha$  stacking or Eq. (B5) for AB- $\beta$  stacking, presented in

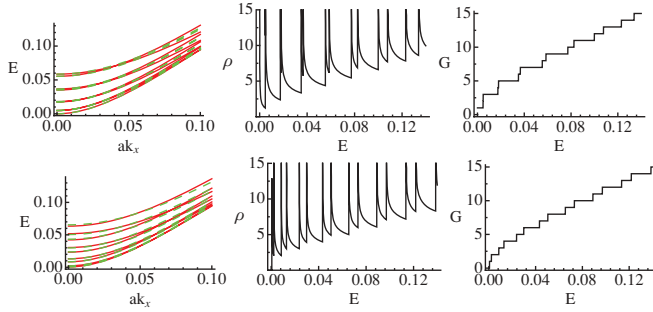


FIG. 7. (Color online) Upper part: band structure of metallic armchair bilayer graphene ribbon with AB- $\alpha$  stacking (left), DOS (center), and conductance (right). The number of hexagons in the  $y$  direction  $N = 101$ . Lower part: band structure of semiconducting armchair bilayer graphene ribbon with AB- $\alpha$  stacking (left), DOS (center), and conductance (right). The number of hexagons in the  $y$  direction  $N = 100$ . Solid red lines are calculated according to Eqs. (44) and (45); dashed green lines represent the approximation calculated with Eq. (73). Bands with  $s_2 = +1$  are not shown. DOS is given in units of  $a^{-1}$  and is calculated according to Eqs. (63) and (74). The conductance is given in units of  $2e^2/h$  and is calculated using Eq. (61).

Appendix B. Since equations for  $\kappa$  depend on the value of the wave vector  $\xi$ , in zigzag bilayer graphene ribbons longitudinal and transverse motions are not separable. When the energy of the subband with the index  $s_2 = -1$  is smaller than the energies of the subbands with index  $s_2 = +1$ , only one of the wave vectors  $\kappa^{(1)}$  and  $\kappa^{(2)}$  has a real value. Therefore, the energy subbands can be labeled by the value of  $\kappa^{(1)} \equiv \kappa_\nu$  only.

Depending on the value of  $|\xi|$ , wave vectors  $\kappa_\nu$  with  $\nu = 0, 1$  can become imaginary. There are two critical values  $\xi^{c(1)}$ ,  $\xi^{c(2)}$  ( $\xi^{c(1)} < \xi^{c(2)}$ ) of the wave vector  $\xi$ , obtained by solving Eqs. (49) and (B1), (B2), or (B5) with  $\kappa^{(1)} = 0$ . When  $\xi^{c(1)} < |\xi| < \xi^{c(2)}$  then one solution  $\kappa_0$  becomes imaginary, whereas in the case  $\xi^{c(2)} < |\xi|$  two solutions,  $\kappa_0$  and  $\kappa_1$ , become imaginary. Both critical values  $\xi^{c(1,2)}$  obey the inequality  $\xi^{c(1,2)} > 2\pi/3$  and tend to the limit  $2\pi/3$  as the number  $N$  grows. A tighter lower bound of critical values is  $\xi^{c(1,2)} > 2 \arccos[N/(2N+1)]$ . The imaginary solutions  $\kappa_\nu$  represent edge states in zigzag bilayer graphene ribbons.

The energy bands of bilayer graphene are asymmetric near the point  $q = 0$ . The subbands (except those corresponding to edge states) can be approximated by taking  $\kappa_\nu \approx \pi\nu/N$  and the minimum of of the subband located at  $\xi^{c(2)}$ :

$$E_\nu(k_y) = s_1 \left\{ -\frac{\gamma}{2} + \sqrt{\frac{\gamma^2}{4} + \frac{9}{4}a^2 \left[ (k_y - \bar{k}_y)^2 + \frac{\pi^2\nu^2}{9a^2N^2} \right]} \right\}, \quad (75)$$

with

$$\bar{k}_y = \frac{\xi^{c(2)}}{\sqrt{3}a}. \quad (76)$$

The critical value  $\xi^{c(2)}$  of the wave vector tends to the limit  $2\pi/3$  as the number  $N$  grows. Conduction (valence) band

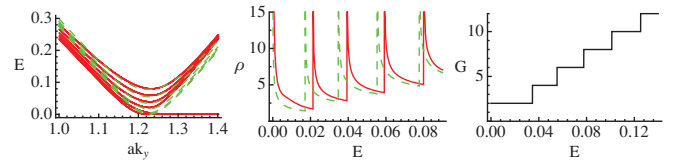


FIG. 8. (Color online) Band structure of zigzag bilayer graphene ribbon with AB- $\alpha$  stacking (left), DOS (center), and conductance (right). The number of rectangular unit cells in the  $x$  direction  $N = 60$ . Solid red lines are calculated according to Eqs. (44) and (45), with the allowed values of the wave vector  $\kappa$  obtained by solving Eqs. (B1), (B2), and (49); dashed green lines represent the approximation of Eq. (75). Bands with  $s_2 = +1$  are not shown. DOS is given in units of  $a^{-1}$ . The conductance is given in units of  $2e^2/h$  and is calculated using Eq. (61).

bottoms (tops) are equal to

$$E_\nu = s_1 \left( -\frac{\gamma}{2} + \sqrt{\frac{\gamma^2}{4} + \frac{\pi^2\nu^2}{4N^2}} \right). \quad (77)$$

The number  $\nu$  of of subbands with the index  $s_2 = -1$  and energy smaller than the energies of the subbands with index  $s_2 = +1$  is greater than 1 only when the number of rectangular unit cells in the  $x$  direction,  $N$ , is sufficiently large. Approximating Eq. (77) as  $\pi^2\nu^2/(4\gamma N^2)$  we get  $N \gg \pi/(2\gamma)$ . In calculations we used  $N = 60$ .

The band structure for zigzag bilayer graphene ribbons with AB- $\alpha$  stacking, calculated using exact Eqs. (44) and (45) with the allowed values of the wave vector  $\kappa$  obtained by solving Eqs. (B1), (B2), and (49), as well as the approximation of Eq. (75), are represented in Fig. 8. Also shown is the DOS and the conductance  $G(E) = (2e^2/h)(2n+2)$ . The DOS is calculated from the exact band structure and also using Eqs. (63) and (74), taking the threshold energies for  $\nu = 0, 1$  to be  $E_{\nu=0,1} = 0$ . The band structure of zigzag bilayer graphene ribbons with AB- $\beta$  stacking is very similar to the band structure of ribbons with AB- $\alpha$  stacking, only the critical values  $\xi^{c(1)}$ ,  $\xi^{c(2)}$  are slightly different.

Taking the limit  $N \rightarrow \infty$  in the zigzag bilayer graphene ribbon with AB- $\beta$  stacking one can obtain the edge states of Ref. 30. However, care should be taken not to lose any solutions. For large  $N$  we can write the absolute value of the imaginary wave vector  $i|\kappa|$  as  $|\kappa| = \kappa^{(0)} + \delta$ , where  $\kappa^{(0)}$  is the solution of the equation

$$e^{-\frac{\kappa^{(0)}}{2}} = 2 \cos(\xi/2), \quad (78)$$

and  $\delta$  is a small correction. From Eq. (44) it follows that such a value of  $\kappa^{(0)}$  ensures the equality  $E(i\kappa^{(0)}, \xi) = 0$ . Expanding Eq. (44) in powers of  $\delta$  we get the approximate expression for the energy

$$E \approx \frac{s_1\delta}{\gamma} \left[ 2 \cos^2\left(\frac{\xi}{2}\right) - \frac{1}{2} \right]. \quad (79)$$

There are two eigenstates with wave vectors  $\kappa^{(1)}$  and  $\kappa^{(2)}$  having different absolute values but corresponding to the same energy. From Eqs. (79) and (48) it follows that the corrections to the wave vector obey the condition

$$\delta^{(2)} = -\delta^{(1)}. \quad (80)$$

In Eq. (B5), taking into account only the first-order terms with respect to  $\delta$ , one obtains the value of the correction

$$\delta = \pm 2e^{-2\kappa^{(0)}N}(1 - e^{-\kappa^{(0)}}). \quad (81)$$

This expression for the correction is the same as for the single sheet of graphene. The correction  $\delta$  decreases exponentially with increasing number  $N$ .

For large  $N$  it is sufficient to form the wave function obeying the boundary conditions of Eq. (47) as a superposition of two exponentially decreasing terms with the wave vectors  $i|\kappa^{(1)}|$  and  $i|\kappa^{(2)}|$ ,

$$\begin{aligned} \psi_{m,n,\alpha_p} = & a^{(1)}c_{\alpha_p}(\xi_j, i|\kappa^{(1)}|)e^{i\xi_j m - |\kappa^{(1)}|n} \\ & + a^{(2)}c_{\alpha_p}(\xi_j, i|\kappa^{(2)}|)e^{i\xi_j m - |\kappa^{(2)}|n}. \end{aligned} \quad (82)$$

Substituting this expression for the wave function in the boundary conditions, using Eqs. (A9)–(A12) and taking the limit  $N \rightarrow \infty$ , we obtain two solutions for the coefficients  $a^{(1)}$ ,  $a^{(2)}$ :  $a^{(2)} = 0$  and  $a^{(2)} = -a^{(1)}$ . The wave function corresponding to the solution  $a^{(2)} = 0$  is localized on the first layer, with the nonzero coefficients  $c_{l_1}$  and  $c_{\rho_1}$ . The wave function corresponding to the solution  $a^{(2)} = -a^{(1)}$  contains the difference  $e^{-|\kappa^{(1)}|n} - e^{-|\kappa^{(2)}|n}$ . Expanding to the first order of  $\delta$  we get

$$e^{-|\kappa^{(1)}|n} - e^{-|\kappa^{(2)}|n} = e^{-(\kappa^{(0)} - \delta)n} - e^{-(\kappa^{(0)} + \delta)n} \approx 2\delta n e^{-\kappa^{(0)}n}. \quad (83)$$

Taking the limit  $N \rightarrow \infty$  and dropping the coefficients of the wave function that are of the order of  $\delta$  we obtain that nonzero coefficients are  $\psi_{m,n,l_1}$ ,  $\psi_{m,n,\rho_1}$  in the first layer and  $\psi_{m,n,r_2}$ ,  $\psi_{m,n,\lambda_2}$  in the second layer. The coefficients  $\psi_{m,n,r_2}$ ,  $\psi_{m,n,\lambda_2}$  are proportional to  $e^{-\kappa^{(0)}n}$  while the coefficients  $\psi_{m,n,l_1}$ ,  $\psi_{m,n,\rho_1}$  have  $ne^{-\kappa^{(0)}n}$  behavior, as in Ref. 30.

## V. CONCLUSIONS

An exact analytical description of  $\pi$  electron spectrum based on the tight-binding model of bilayer graphene has been presented. The bilayer graphene structures considered in this article have rectangular geometry and finite size in one or both directions with armchair- and zigzag-shaped edges. This includes bilayer graphene nanoribbons and nanotubes. The exact solution of the Schrödinger problem, the spectrum and wave functions, has been obtained and used to analyze the density of states and the conductance quantization. Our method illustrates a connection between  $\pi$ -electron spectra in infinite and finite-sized bilayer graphene.

## ACKNOWLEDGMENTS

The authors acknowledge a collaborative grant from the Swedish Institute and Grant No. MIP-123/2010 by the Research Council of Lithuania. I.V.Z. acknowledges support from the Swedish Research Council (VR).

## APPENDIX A: EIGENVECTORS OF BILAYER GRAPHENE USING RECTANGULAR UNIT CELLS

The expressions for the coefficients of the eigenvectors are: For AB- $\alpha$  stacking,  $V = 0$ ,

$$c_{r_1} = 1, \quad c_{\rho_1} = -e^{-i\frac{\kappa}{2}} \frac{E(\kappa, \xi)}{\phi(-\kappa, \xi)}, \quad (A1)$$

$$c_{l_1} = -s_3 e^{-i\frac{\kappa}{2}} \frac{E(\kappa, \xi)}{\phi(-\kappa, \xi)}, \quad c_{\lambda_1} = s_3 e^{-i\frac{1}{2}(\kappa + \xi)}, \quad (A2)$$

$$c_{r_2} = -s_1 s_2 \frac{\phi(\kappa, \xi)}{\phi(-\kappa, \xi)}, \quad c_{\rho_2} = s_1 s_2 e^{-i\frac{\kappa}{2}} \frac{E(\kappa, \xi)}{\phi(-\kappa, \xi)}, \quad (A3)$$

$$c_{l_2} = s_1 s_2 s_3 e^{i\frac{\kappa}{2}} \frac{E(\kappa, \xi)}{\phi(-\kappa, \xi)}, \quad (A4)$$

$$c_{\lambda_2} = -s_1 s_2 s_3 e^{i\frac{1}{2}(\kappa - \xi)} \frac{\phi(\kappa, \xi)}{\phi(-\kappa, \xi)}.$$

For AB- $\alpha$  stacking,  $V \neq 0$ ,

$$c_{r_1} = 1, \quad c_{\rho_1} = -e^{-i\frac{\kappa}{2}} \frac{E + V}{\phi(-\kappa, \xi)}, \quad (A5)$$

$$c_{l_1} = -s_3 e^{-i\frac{\kappa}{2}} \frac{E + V}{\phi(-\kappa, \xi)}, \quad c_{\lambda_1} = s_3 e^{-i\frac{1}{2}(\kappa + \xi)}, \quad (A6)$$

$$c_{r_2} = -\frac{\phi(\kappa, \xi)}{\phi(-\kappa, \xi)} f(\kappa, \xi), \quad (A7)$$

$$c_{\rho_2} = s_1 s_2 e^{-i\frac{\kappa}{2}} \frac{E - V}{\phi(-\kappa, \xi)} f(\kappa, \xi),$$

$$c_{l_2} = s_1 e^{i\frac{\kappa}{2}} \frac{E - V}{\phi(-\kappa, \xi)} f(\kappa, \xi), \quad (A8)$$

$$c_{\lambda_2} = -s_3 e^{i\frac{1}{2}(\kappa - \xi)} \frac{\phi(\kappa, \xi)}{\phi(-\kappa, \xi)} f(\kappa, \xi).$$

For AB- $\beta$  stacking,  $V = 0$ ,

$$c_{r_1} = 1, \quad c_{\rho_1} = -e^{-i\frac{\kappa}{2}} \frac{\phi(\kappa, \xi)}{E(\kappa, \xi)}, \quad (A9)$$

$$c_{l_1} = -s_3 e^{-i\frac{\kappa}{2}} \frac{\phi(\kappa, \xi)}{E(\kappa, \xi)}, \quad c_{\lambda_1} = s_3 e^{-i\frac{1}{2}(\kappa + \xi)}, \quad (A10)$$

$$c_{r_2} = -s_1 s_2 s_3 e^{i\frac{1}{2}(\xi - \kappa)}, \quad c_{\rho_2} = s_1 s_2 s_3 e^{-i\frac{\kappa}{2}} \frac{\phi(-\kappa, \xi)}{E(\kappa, \xi)}, \quad (A11)$$

$$c_{l_2} = s_1 s_2 e^{i\frac{\kappa}{2}} \frac{\phi(-\kappa, \xi)}{E(\kappa, \xi)}, \quad c_{\lambda_2} = -s_1 s_2. \quad (A12)$$

For AB- $\beta$  stacking,  $V \neq 0$ ,

$$c_{r_1} = 1, \quad c_{\rho_1} = -e^{-i\frac{\kappa}{2}} \frac{\phi(\kappa, \xi)}{E + V}, \quad (A13)$$

$$c_{l_1} = -s_3 e^{-i\frac{\kappa}{2}} \frac{\phi(\kappa, \xi)}{E + V}, \quad c_{\lambda_1} = s_3 e^{-i\frac{1}{2}(\kappa + \xi)}, \quad (A14)$$

$$c_{r_2} = -s_3 e^{i\frac{1}{2}(\xi - \kappa)} f(\kappa, \xi), \quad (\text{A15})$$

$$c_{\rho_2} = s_3 e^{-i\frac{\xi}{2}} \frac{\phi(-\kappa, \xi)}{E - V} f(\kappa, \xi),$$

$$c_{l_2} = s_1 s_2 e^{i\frac{\xi}{2}} \frac{\phi(-\kappa, \xi)}{E - V} f(\kappa, \xi), \quad c_{\lambda_2} = -f(\kappa, \xi). \quad (\text{A16})$$

## APPENDIX B: WAVE VECTORS OF ZIGZAG BILAYER CARBON TUBES

For AB- $\alpha$  stacking and  $V = 0$ , the possible values of  $\kappa_{j,v_j}^{(1)}$  are solutions of one of the equations

$$1 + \cos\left(\frac{\xi}{2}\right) \left\{ s_3^{(1)} \frac{\cos\left[\frac{1}{2}\kappa^{(1)}(N+1)\right]}{\cos\left[\frac{1}{2}\kappa^{(1)}N\right]} + s_3^{(2)} \frac{\sin\left[\frac{1}{2}\kappa^{(2)}(N+1)\right]}{\sin\left[\frac{1}{2}\kappa^{(2)}N\right]} \right\} = 0 \quad (\text{B1})$$

or

$$1 + \cos\left(\frac{\xi}{2}\right) \left\{ s_3^{(1)} \frac{\sin\left[\frac{1}{2}\kappa^{(1)}(N+1)\right]}{\sin\left[\frac{1}{2}\kappa^{(1)}N\right]} + s_3^{(2)} \frac{\cos\left[\frac{1}{2}\kappa^{(2)}(N+1)\right]}{\cos\left[\frac{1}{2}\kappa^{(2)}N\right]} \right\} = 0. \quad (\text{B2})$$

When  $V \neq 0$ , then the equation for  $\kappa$  reads

$$\begin{aligned} & \frac{1}{4} [f(\kappa^{(1)}) - f(\kappa^{(2)})]^2 \left\{ 1 + 2s_3^{(1)} \cos\left(\frac{\xi}{2}\right) \frac{\sin\left[\kappa^{(1)}\left(N + \frac{1}{2}\right)\right]}{\sin[\kappa^{(1)}N]} \right\} \left\{ 1 + 2s_3^{(2)} \cos\left(\frac{\xi}{2}\right) \frac{\sin\left[\kappa^{(2)}\left(N + \frac{1}{2}\right)\right]}{\sin[\kappa^{(2)}N]} \right\} \\ & - f(\kappa^{(1)})f(\kappa^{(2)}) \cos^2\left(\frac{\xi}{2}\right) \left\{ s_3^{(1)} \frac{\cos\left[\frac{1}{2}\kappa^{(1)}(N+1)\right]}{\cos\left[\frac{1}{2}\kappa^{(1)}N\right]} - s_3^{(2)} \frac{\cos\left[\frac{1}{2}\kappa^{(2)}(N+1)\right]}{\cos\left[\frac{1}{2}\kappa^{(2)}N\right]} \right\} \\ & \times \left\{ s_3^{(1)} \frac{\sin\left[\frac{1}{2}\kappa^{(1)}(N+1)\right]}{\sin\left[\frac{1}{2}\kappa^{(1)}N\right]} - s_3^{(2)} \frac{\sin\left[\frac{1}{2}\kappa^{(2)}(N+1)\right]}{\sin\left[\frac{1}{2}\kappa^{(2)}N\right]} \right\} = 0. \end{aligned} \quad (\text{B3})$$

Here the function

$$f(\kappa, \xi) = \frac{(E + V)^2 - |\phi(\kappa, \xi)|^2}{\gamma(E - V)} \quad (\text{B4})$$

describes the contribution of the second sheet of graphene to the eigenvector.

For AB- $\beta$  stacking and  $V = 0$ , the possible values of  $\kappa$  are solutions of the equation

$$\begin{aligned} & \left\{ 1 + 2s_3^{(1)} \cos\left(\frac{\xi}{2}\right) \frac{\sin\left[\kappa^{(1)}\left(N + \frac{1}{2}\right)\right]}{\sin[\kappa^{(1)}N]} \right\} \left\{ 1 + 2s_3^{(2)} \cos\left(\frac{\xi}{2}\right) \frac{\sin\left[\kappa^{(2)}\left(N + \frac{1}{2}\right)\right]}{\sin[\kappa^{(2)}N]} \right\} \\ & + \frac{1}{2} s_3^{(1)} s_3^{(2)} \left\{ \cos\left[\frac{\kappa^{(1)}}{2}\right] \cos\left[\frac{\kappa^{(2)}}{2}\right] + \frac{1 - \cos[\kappa^{(1)}N] \cos[\kappa^{(2)}N]}{\sin[\kappa^{(1)}N] \sin[\kappa^{(2)}N]} \sin\left[\frac{\kappa^{(1)}}{2}\right] \sin\left[\frac{\kappa^{(2)}}{2}\right] \right\} - \frac{1}{2} = 0. \end{aligned} \quad (\text{B5})$$

When  $V \neq 0$ , then the equation for  $\kappa$  is

$$\begin{aligned} & \frac{1}{4} [f(\kappa^{(1)}) - f(\kappa^{(2)})]^2 \left\{ 1 + 2s_3^{(1)} \cos\left(\frac{\xi}{2}\right) \frac{\sin\left[\kappa^{(1)}\left(N + \frac{1}{2}\right)\right]}{\sin[\kappa^{(1)}N]} \right\} \left\{ 1 + 2s_3^{(2)} \cos\left(\frac{\xi}{2}\right) \frac{\sin\left[\kappa^{(2)}\left(N + \frac{1}{2}\right)\right]}{\sin[\kappa^{(2)}N]} \right\} \\ & + \frac{1}{2} f[\kappa^{(1)}]f[\kappa^{(2)}] \left\{ 1 - s_3^{(1)} s_3^{(2)} \left[ \cos\left(\frac{\kappa^{(1)}}{2}\right) \cos\left(\frac{\kappa^{(2)}}{2}\right) + \frac{1 - \cos(\kappa^{(1)}N) \cos(\kappa^{(2)}N)}{\sin(\kappa^{(1)}N) \sin(\kappa^{(2)}N)} \sin\left(\frac{\kappa^{(1)}}{2}\right) \sin\left(\frac{\kappa^{(2)}}{2}\right) \right] \right\} = 0 \end{aligned} \quad (\text{B6})$$

\*julius.ruseckas@fai.vu.lt; [http://www.itpa.lt/~ruseckas]

<sup>1</sup>A. H. Castro Neto, F. Guinea, N. M. R. Peres, K. S. Novoselov, and A. K. Geim, *Rev. Mod. Phys.* **81**, 109 (2009).

<sup>2</sup>D. S. L. Abergela, V. Apalkov, J. Berashevich, K. Ziegler, and T. Chakraborty, *Adv. Phys.* **59**, 261 (2010).

<sup>3</sup>S. D. Sarma, S. Adam, E. H. Hwang, and E. Rossi, *Rev. Mod. Phys.* (2010), to be published, e-print [arXiv:1003.4731v1](https://arxiv.org/abs/1003.4731v1) [cond-mat.mes-hall].

<sup>4</sup>N. M. R. Peres, *Rev. Mod. Phys.* **82**, 2673 (2010).

<sup>5</sup>X. Du, I. Skachko, A. Barker, and E. Y. Andrei, *Nature Nanotech.* **3**, 491 (2008).

<sup>6</sup>E. McCann, *Phys. Rev. B* **74**, 161403(R) (2006).

- <sup>7</sup>J. B. Oostinga, H. B. Heersche, X. Liu, A. F. Morpurgo, and L. M. K. Vandersypen, *Nat. Mater.* **7**, 151 (2007).
- <sup>8</sup>F. Xia, D. B. Farmer, Y. Lin, and P. Avouris, *Nano. Lett.* **10**, 715 (2010).
- <sup>9</sup>K. Wakabayashi, M. Fujita, H. Ajiki, and M. Sigrist, *Phys. Rev. B* **59**, 8271 (1999).
- <sup>10</sup>Y.-W. Son, M. L. Cohen, and S. G. Louie, *Phys. Rev. Lett.* **97**, 216803 (2006).
- <sup>11</sup>M. Y. Han, B. Özyilmaz, Y. Zhang, and P. Kim, *Phys. Rev. Lett.* **98**, 206805 (2007).
- <sup>12</sup>Y.-M. Lin, V. Perebeinos, Z. Chen, and P. Avouris, *Phys. Rev. B* **78**, 161409(R) (2008).
- <sup>13</sup>M. Ewaldsson, I. V. Zozoulenko, H. Xu, and T. Heinzel, *Phys. Rev. B* **78**, 161407 (2008).
- <sup>14</sup>E. R. Mucciolo, A. H. Castro Neto, and C. H. Lewenkopf, *Phys. Rev. B* **79**, 075407 (2009).
- <sup>15</sup>S. Ihnatsenka and G. Kirczenow, *Phys. Rev. B* **80**, 201407 (2009).
- <sup>16</sup>X. Jia *et al.*, *Science* **323**, 1701 (2009).
- <sup>17</sup>D. V. Kosynkin, A. L. Higginbotham, A. Sinitskii, J. R. Lomeda, A. Dimiev, B. K. Price, and J. M. Tour, *Nature (London)* **458**, 872 (2009).
- <sup>18</sup>L. Jiao, L. Zhang, X. Wang, G. Diankov, and H. Dai, *Nature (London)* **458**, 877 (2009).
- <sup>19</sup>X. Li, X. Wang, L. Zhang, S. Lee, and H. Dai, *Science* **319**, 1229 (2008).
- <sup>20</sup>J. Cai *et al.*, *Nature (London)* **466**, 470 (2010).
- <sup>21</sup>L. Brey and H. A. Fertig, *Phys. Rev. B* **73**, 235411 (2006).
- <sup>22</sup>H. Zheng, Z. F. Wang, T. Luo, Q. W. Shi, and J. Chen, *Phys. Rev. B* **75**, 165414 (2007).
- <sup>23</sup>L. Malysheva and A. I. Onipko, *Phys. Rev. Lett.* **100**, 186806 (2008).
- <sup>24</sup>A. Onipko, *Phys. Rev. B* **78**, 245412 (2008).
- <sup>25</sup>L. Jiang, Y. Zheng, C. Yi, H. Li, and T. Lü, *Phys. Rev. B* **80**, 155454 (2009).
- <sup>26</sup>F. Guinea, A. H. Castro Neto, and N. M. R. Peres, *Phys. Rev. B* **73**, 245426 (2006).
- <sup>27</sup>B. Partoens and F. M. Peeters, *Phys. Rev. B* **74**, 075404 (2006).
- <sup>28</sup>Z. F. Wang, Q. Li, H. Su, X. Wang, Q. W. Shi, J. Chen, J. Yang, and J. G. Hou, *Phys. Rev. B* **75**, 085424 (2007).
- <sup>29</sup>J. Nilsson, A. H. Castro Neto, F. Guinea, and N. M. R. Peres, *Phys. Rev. B* **78**, 045405 (2008).
- <sup>30</sup>E. V. Castro, N. M. R. Peres, J. M. B. Lopes dos Santos, A. H. Castro Neto, and F. Guinea, *Phys. Rev. Lett.* **100**, 026802 (2008).
- <sup>31</sup>H. Xu, T. Heinzel, and I. V. Zozoulenko, *Phys. Rev. B* **80**, 045308 (2009).
- <sup>32</sup>H. Xu, T. Heinzel, A. A. Shylau, and I. V. Zozoulenko, *Phys. Rev. B* **82**, 115311 (2010).
- <sup>33</sup>E. V. Castro, N. M. R. Peres, and J. M. B. Lopes dos Santos, *Europhys. Lett.* **84**, 17001 (2008).
- <sup>34</sup>R. Landauer, *IBM J. Res. Dev.* **1**, 233 (1957).
- <sup>35</sup>R. Landauer, *IBM J. Res. Dev.* **32**, 306 (1988).
- <sup>36</sup>M. Büttiker, *Phys. Rev. Lett.* **57**, 1761 (1986).
- <sup>37</sup>M. Büttiker, *Phys. Rev. B* **38**, 9375 (1988).